

REVIEW ARTICLE

Open Access



Micromechanical and Ultrastructural Properties of Abdominal Aortic Aneurysms

Martin Hossack^{1,2*} , Robert Fisher², Francesco Torella², Jillian Madine³, Mark Field⁴ and Riaz Akhtar¹

Abstract

Abdominal aortic aneurysms are a common condition of uncertain pathogenesis that can rupture if left untreated. Current recommended thresholds for planned repair are empirical and based entirely on diameter. It has been observed that some aneurysms rupture before reaching the threshold for repair whilst other larger aneurysms do not rupture. It is likely that geometry is not the only factor influencing rupture risk. Biomechanical indices aiming to improve and personalise rupture risk prediction require, amongst other things, knowledge of the material properties of the tissue and realistic constitutive models. These depend on the composition and organisation of the vessel wall which has been shown to undergo drastic changes with aneurysmal degeneration, with loss of elastin, smooth muscle cells, and an accumulation of isotropically arranged collagen. Most aneurysms are lined with intraluminal thrombus, which has an uncertain effect on the underlying vessel wall, with some authors demonstrating a reduction in wall stress and others a reduction in wall strength. The majority of studies investigating biomechanical properties of ex vivo abdominal aortic aneurysm tissues have used low-resolution techniques, such as tensile testing, able to measure the global material properties at the macroscale. High-resolution engineering techniques such as nanoindentation and atomic force microscopy have been modified for use in soft biological tissues and applied to vascular tissues with promising results. These techniques have the potential to advance the understanding and improve the management of abdominal aortic aneurysmal disease.

Keywords: Abdominal aortic aneurysm, Intraluminal thrombus, Ultrastructure, Micromechanics, Nanoindentation, Atomic force microscopy, Elastic modulus

1 Background

Abdominal aortic aneurysms (AAAs) are found in 1.3–5.7% of the male population over the age of 65 [1]. They are usually asymptomatic prior to rupture, following which the mortality is 50–90% [2]. Open surgical repair (OSR), which involves replacement of the diseased segment with a prosthetic graft, has an early mortality of 3.2%, whilst following endovascular aneurysm repair (EVAR), in which a self-expanding stent graft is deployed under imaging guidance via the femoral arteries, it is 1.2% [3]. Planned repair is usually delayed until the risk

of aneurysm rupture exceeds the risks associated with repair. Necropsy and clinical studies have indicated that the risk of rupture accelerates with increasing diameter [4]. The current recommended and most widely utilised threshold for repair is based on geometry. That is, when the maximum aneurysm diameter exceeds 5.5 cm in men and 5 cm in women or increases by > 1 cm/year [5]. Whilst delaying repair until these empirical thresholds are reached has been shown to be as safe as early repair for a population [6], autopsy studies have shown that small AAAs do rupture [7], and in certain instances large aneurysms will not rupture given the life-expectancy of the patient. Furthermore, not all aneurysms enlarge at the same rate [8], with the potential for faster growing

*Correspondence: m.hossack@liverpool.ac.uk

¹ Mechanical, Materials and Aerospace Engineering, University of Liverpool, Liverpool, UK

Full list of author information is available at the end of the article



© The Author(s) 2022. **Open Access** This article is licensed under a Creative Commons Attribution 4.0 International License, which permits use, sharing, adaptation, distribution and reproduction in any medium or format, as long as you give appropriate credit to the original author(s) and the source, provide a link to the Creative Commons licence, and indicate if changes were made. The images or other third party material in this article are included in the article's Creative Commons licence, unless indicated otherwise in a credit line to the material. If material is not included in the article's Creative Commons licence and your intended use is not permitted by statutory regulation or exceeds the permitted use, you will need to obtain permission directly from the copyright holder. To view a copy of this licence, visit <http://creativecommons.org/licenses/by/4.0/>.

aneurysms to rupture whilst under surveillance or awaiting repair.

Biomechanically, AAA rupture occurs when stress acting upon the wall overcomes the strength of the wall to resist this stress. The predominant source of stress is systemic pressurisation, which is orders of magnitude larger than the shear stress due to blood flow across the wall. The theoretical basis for utilising the maximum diameter to predict wall stress is the Law of Laplace. This states that the wall stress of a thin-walled sphere is proportional to its diameter. However, this cannot account for complex geometry as is seen in AAA. Using realistic geometry, it can be seen that different parts of a given AAA's wall will display significantly different wall stresses [9, 10] and two aneurysms with identical maximum diameters can have significantly different wall stress distributions (Fig. 1).

To improve and personalise AAA rupture risk prediction, biomechanically based models have been developed which include a quantification of individual wall stress using the finite element analysis (FEA) method [11]. This

requires information regarding the material properties of the tissues, as well as aortic geometry, wall thickness, applied forces, boundary conditions, and use of appropriate constitutive models [2]. Using these methods, it has been demonstrated that peak wall stress (PWS) is significantly higher in symptomatic and ruptured, than electively repaired AAAs [9]; PWS is superior to maximum diameter in predicting rupture or development of symptoms [10]; and PWS correlates to the site of AAA rupture [12]. Improving our understanding of the material properties of AAA tissue has the potential to improve rupture risk prediction. These properties are determined by the composition and organisation of the tissue. In Sect. 2, we summarise the structural changes in the vessel wall occurring with aneurysmal dilatation. In Sect. 3 we review the mechanical testing of AAA wall tissue at different length scales, focusing on novel applications of high-resolution engineering techniques. Intraluminal thrombus tissue (ILT) lines most AAAs and has been shown to affect the underlying aortic wall in a variety of

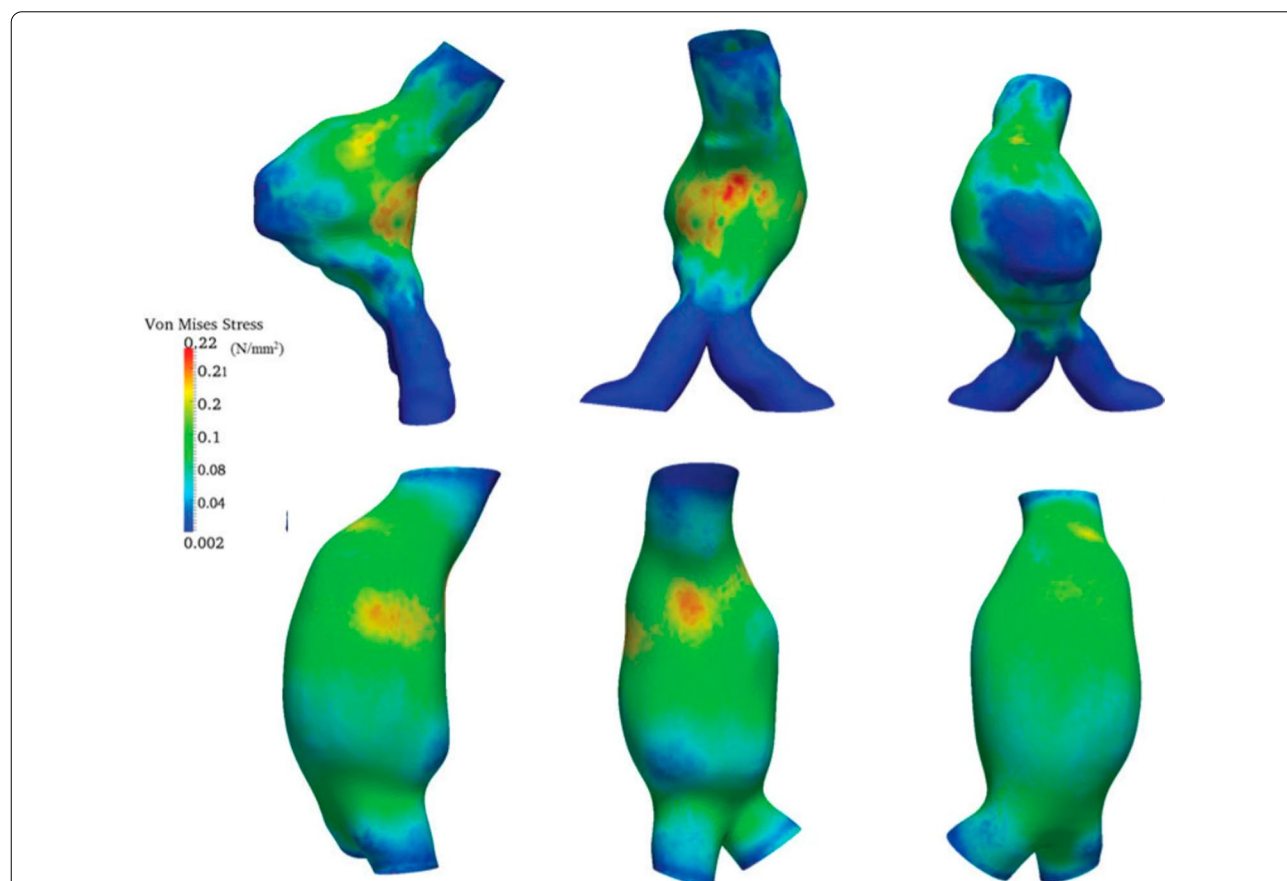


Fig. 1 Von Mises stress distribution in two AAA's. The top images demonstrate a AAA with a focal area of high stress in the posterior wall. The bottom images demonstrate a AAA with a more uniform wall stress distribution. © 1999 Nikolaos Kontopodis, Konstantinos Tzirakis, Emmanouil Tavlas, Stella Lioudaki and Christos Ioannou. Originally published in Abdominal Aortic Aneurysm—From Basic Research to Clinical Practice under CC BY-NC 4.0 license. Available from: <http://dx.doi.org/10.5772/intechopen.76121>

ways. In Sect. 4, we review the structure and mechanical testing of ILT.

2 Structural Changes in AAA Wall

2.1 Biochemistry

The aorta comprises of cellular components embedded in an extracellular matrix (ECM), which provides the structural and mechanical function. The cellular components consist of endothelial cells, which line and interact with the flow lumen; smooth muscle cells (SMCs) and fibroblasts, which are responsible for synthesising and organising the ECM. The ECM consists mainly of the fibrillar proteins elastin and collagen, which are organised into fibres. They are predominantly responsible for the mechanical properties of the aorta, providing passive elastic recoil and tensile strength, respectively. They constitute ~50% of the dry weight of large arteries such as the aorta [13]. The ECM also contains proteoglycans (PGs), glycoproteins and glycosaminoglycans (GAGs). The principle PG in the aorta is versican, which interacts with hyaluronan—one of the three GAGs found in the aorta—to form aggregates that trap water, creating viscoelastic and turgor pressure, possibly preventing deformation of the vessel wall and compression of the cellular components, by the pulsatile pressure within the lumen [14].

The composition of the aorta changes as it becomes aneurysmal. There is a well-established drastic loss of elastin and SMCs, and a compensatory increase in collagen concentration [15]. Reductions in the amount of PG [14], GAG [16], and numerous other ECM proteins [17] have also been demonstrated. These changes are mediated by unregulated proteinase activity, an explanation of which is beyond the scope of this review.

2.2 Architecture

2.2.1 Healthy Aorta

The aorta is a hierarchical structure that can be divided into three layers—intima, media and adventitia—separated by internal and external elastic lamellae. In healthy tissue, each of these layers is distinct. The intima (innermost) consisting of a single layer of endothelial cells, is mechanically insignificant in young healthy vessels but stiffens with age [18–20]. The media is the thickest and most mechanically significant layer. It consists of a series of concentric subunits—medial lamellar units (MLUs)—comprising elastin, SMCs and collagen [21]. Elastin is found in three forms: thick continuous circumferentially orientated sheets (lamellae), which are the main load-bearing layer at physiological loads [22]; dense interlamellar fibres, which protrude obliquely from lamellae to surround the SMCs, facilitating mechanotransduction [23]; and radially

orientated struts connecting adjacent lamellae, providing support for radial loads, preventing delamination or dissection (Fig. 2).

Scanning electron microscopy (SEM) images of healthy *ascending* aortic tissue reveal the elastic lamellae to be perforated by irregular pores (Fig. 3A), which may allow radial passage of metabolites across the aortic wall. The lamellae are themselves formed from a coalescence of fibrillary components running in small bundles, and their surface is characterised by protrusions of fibrous fascicles extending into the interlamellar space (Fig. 3B) [24].

Collagen is found in all layers of the aortic wall. The orientation of the fibres is layer-specific with no fibres passing in the radial direction. In the intima and media, fibres are predominantly circumferential (Fig. 4, Healthy, panes I, M); and in the adventitia, axial (Fig. 4, Healthy, pane A). Transition zones between intima–media and media–adventitia represent the internal and external elastic laminae, respectively [18].

At unloaded and physiological pressures adventitial collagen fibres appear wavy [18], straightening at higher pressures, preventing over-stretch and rupture, producing the characteristic non-linear stress–strain curve seen in healthy arteries. Collagen is organised in thin uniform fibrils gathered into bundles, with individual fibrils connected by small proteoglycans (Fig. 5) [24].

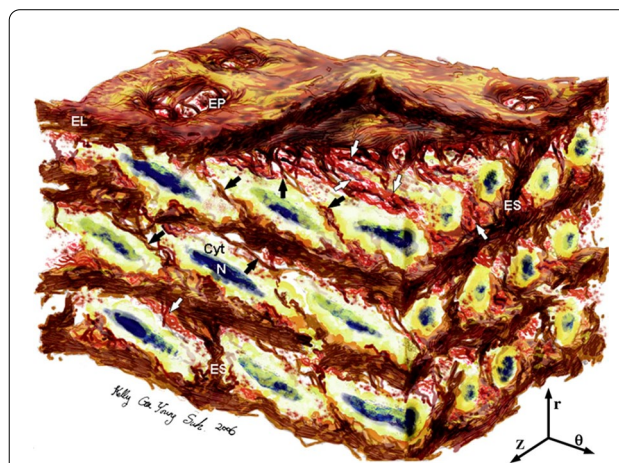


Fig. 2 Artistic rendering of 3D medial aortic microstructure demonstrating the concentric medial lamellar units consisting of parallel Elastic Lamellae (EL), perforated by Elastin Pores (EP) and interconnected by Elastin Struts (ES). The interlamellar zones contain smooth muscle cells whose elliptical nuclei (N) are orientated circumferentially and whose cytoplasm (Cyt) abuts interlamellar elastin fibres (black arrows), which transmit mechanical forces to the cells. Collagen fibres (white arrows) are adjacent to lamellar surfaces and are orientated predominantly circumferentially. Reprinted from O’Connell et al. [21] with permission from Elsevier

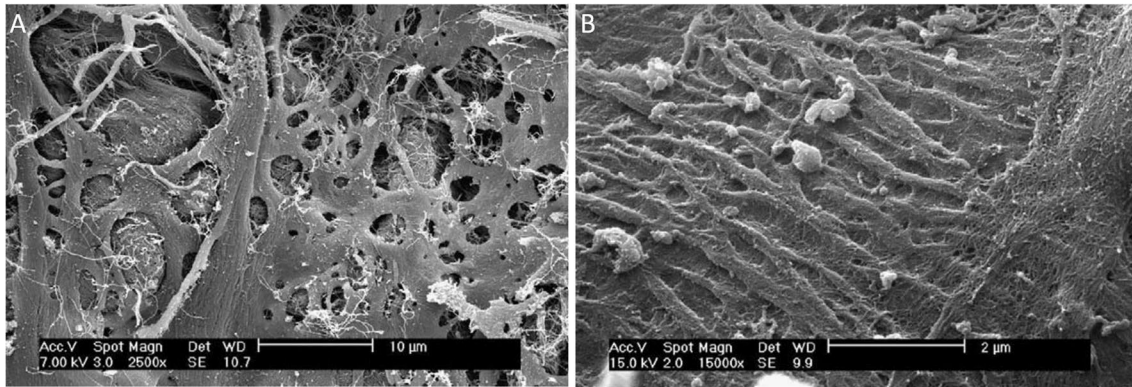


Fig. 3 Scanning electron microscopy (SEM) images of human ascending aortic aneurysm tissue at increasing magnification, demonstrating; **A** Web-like elastic fibre showing irregular holes, through which collagen fibres can be seen; **B** Elastic lamellar surface consisting of coalesced fibrils in bundles. Adapted from Raspanti et al. [24] with permission from Elsevier

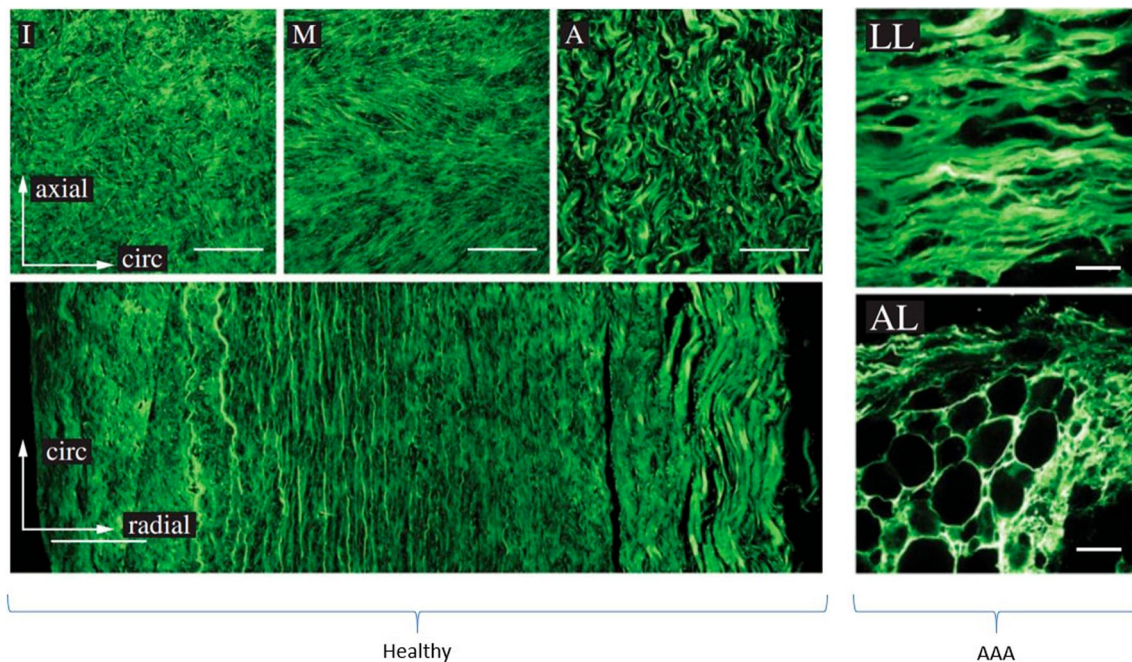


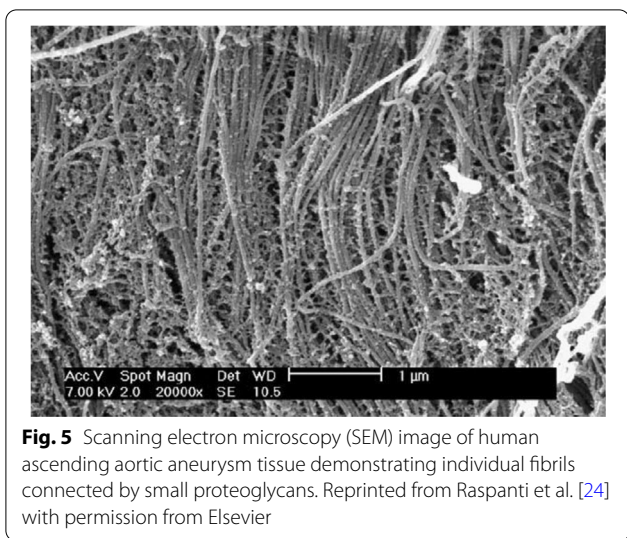
Fig. 4 Second-harmonic generation (SHG) images of: (left) a healthy abdominal aorta. Top three images: in-plane sections of the intima (I), media (M) and adventitia (A). Bottom image: Image through whole thickness of vessel, intima towards left hand side of image, adventitia to the right. (Right) tissue taken from a ruptured abdominal aortic aneurysm. Top image: LL Luminal Layer demonstrating orientation of collagen fibres towards the circumferential direction. Bottom image: AL Abluminal Layer demonstrating marked adipocyte deposition and cystic medial degeneration. μ Scale bar, 100 μ m. Used with permission of Royal Society (Great Britain), from Niestrawska et al. [18]; permission conveyed through Copyright Clearance Center, Inc

2.2.2 Aneurysmal Aorta

AAA tissue is characterised by loss of the normal three-layer distinction. There is substantial variability in fibre architecture, even between samples from the same aneurysm, and a marked reorientation of collagen fibres

into the circumferential direction. Towards the abluminal side, there is adipocyte deposition and cystic medial degeneration (Fig. 4, AAA panes) [18].

Niestrawska et al. measured collagen fibre orientation in AAA tissue, grouping samples according to their

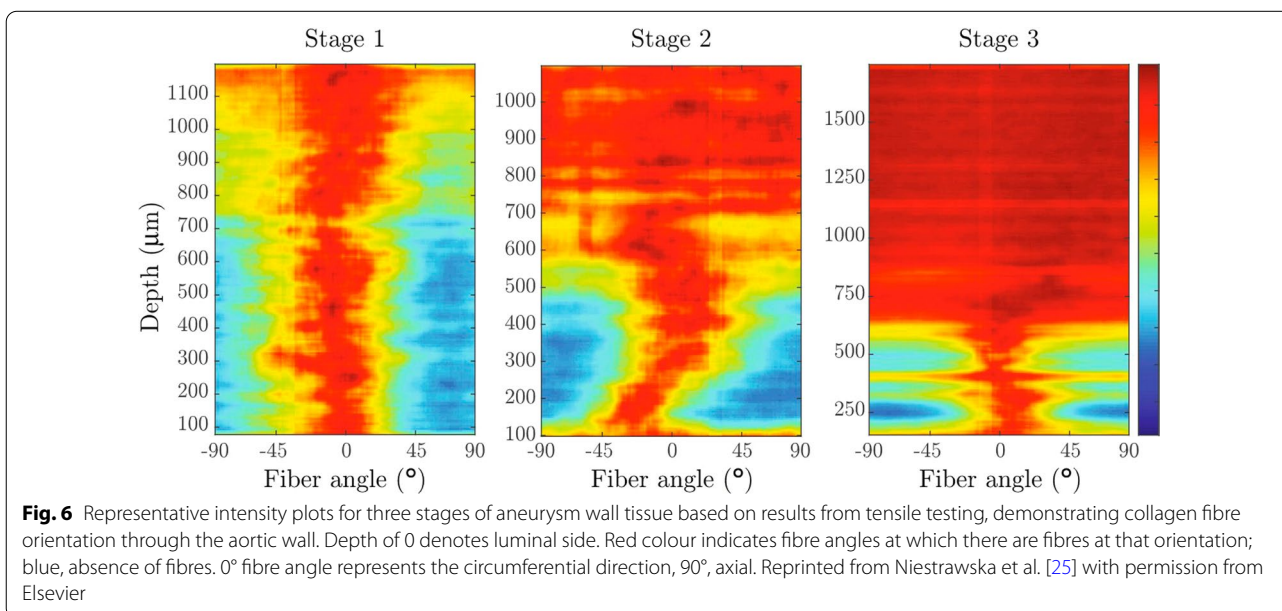


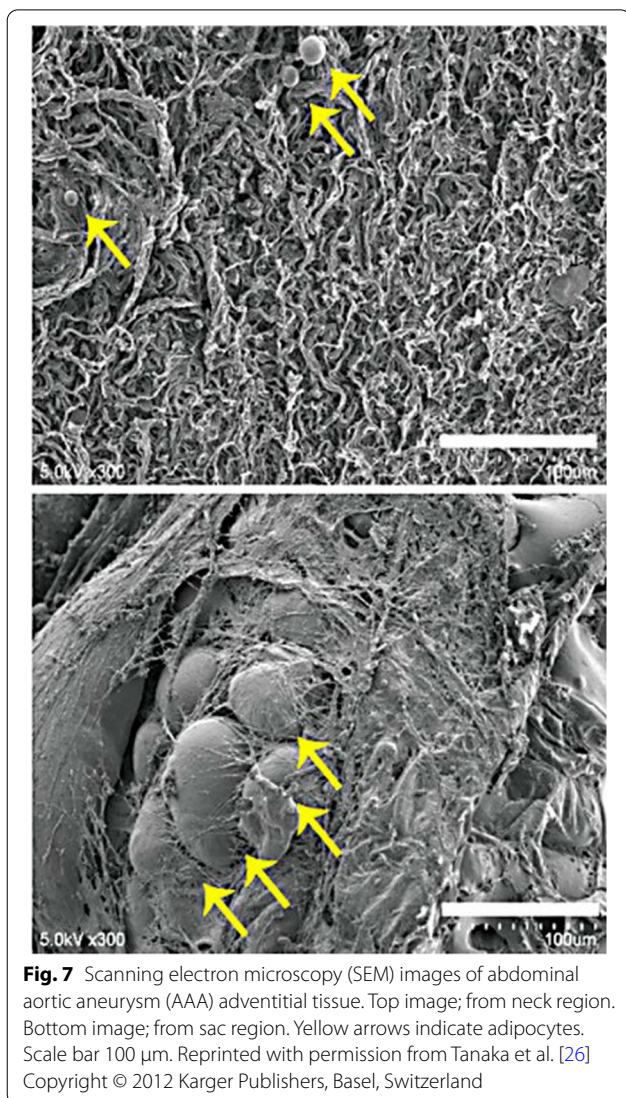
relationship with a healthy ‘inflection point’, indicating rapid stiffening and therefore collagen recruitment, established by tensile testing [25]. All samples demonstrated drastic reductions in elastin and SMC content. In stage 1 (healthy inflection point) samples there was a marked reorientation of collagen fibres to a circumferential direction (Fig. 6, left). Stage 2 (more distensible) samples were characterised by an accumulation of isotropically dispersed collagen peripherally (Fig. 6, centre). Stage 3 (less distensible) samples demonstrated a significantly thickened layer of isotropically dispersed collagen comprising a median 66.22% of the wall thickness (Fig. 6,

right). Nerves normally seen in the periadventitial tissue could be found embedded in this ‘neo-adventitia’. Within stage 3, two distinct morphologies were noted: The ‘safely remodelled’ subgroup consisted of a thick layer of collagen entrapping nerves, with no visible adipocytes. Whereas the ‘vulnerable’ group demonstrated significant amounts of inflammation and adipocytes. No difference in the median diameters of safe and vulnerable AAAs was seen, reinforcing the theory that maximum diameter alone is insufficient to characterise an individual’s rupture risk.

The presence of triglyceride (TG) molecules in the adventitia has been shown to be much higher in AAA sac than neck tissue, as demonstrated by Tanaka et al. using a matrix-assisted laser desorption/ionisation imaging mass spectrometry (MALDI-IMS) imaging system [26]. This system allows characterisation of molecules on vascular tissue sections without requiring antibodies or staining. TG’s were found within ectopic adipocytes, which were much larger in the sac region. The collagen fibres here were thinner and displayed a more irregular structure (Fig. 7). High circulating TG levels have been implicated as a risk factor for aneurysm rupture [27]. The accumulation of TG within adipocytes located in the adventitia may lead to adipocyte hypertrophy and disruption of the ECM collagen network, so crucial to resist over-stretching and rupture.

Majewski et al. examined the ultrastructure of tissue from the non-dilated neck and sac of infra-renal AAA patients with transmission electron microscopy [28]. Patients were grouped according to subsequent neck





dilatation during follow-up. Tissue from patients with subsequent minor dilatation (median 1 mm increase) demonstrated minimal disorganisation in the aortic neck wall. The media demonstrated a normal arrangement of elastin fibres, collagen and SMCs. The adventitia was composed of regular fibroblasts surrounded by collagen fibres, proteoglycans and glycosaminoglycans. Tissue from patients with increased neck dilatation (median 5.2 mm increase) demonstrated partially disrupted elastic fibres, haphazardly organised collagen bundles and inflammatory cell infiltrates. Ultrastructural findings correlated with pre-operative distensibility measured by motion-mode ultrasound (US)—neck tissue from more distensible aorta demonstrated less severe ultrastructural changes and underwent less subsequent dilatation, and vice versa. Unsurprisingly aneurysm sac tissue displayed

the most severe changes. Large areas without endothelial lining were seen. Elastic fibres were either, fragmented and surrounded by necrotic cells, or totally absent. Areas of the media contained haphazardly arranged collagen fibres and glycosaminoglycans. Other areas were acellular with no visible SMCs. Monocyte/macrophages, lymphoid cells and erythrocytes were seen, with some macrophages containing lipid. The fibrillary structures were completely without organisation [28].

3 Mechanical Testing of AAA Wall

3.1 Macroscale

A detailed account of the macroscale mechanical testing of aortic tissue is beyond the scope of this review. We have summarised the most important findings from the main modalities of *in vivo* and *ex vivo* mechanical testing.

3.1.1 *In Vivo* Testing

Ejection of blood from the left ventricle induces a wave that propagates through the arterial tree, causing distensibility of the vessel wall. The speed of this wave, pulse wave velocity (PWV), has been used to measure arterial stiffness in patients with AAA, finding they had significantly higher PWV (higher stiffness), with a less uniform pulse wave propagation [29]. Van Disseldorp et al. used time-resolved three-dimensional (3D) US to track aortic wall motion during systole and diastole in healthy and AAA patients. Simulated displacements generated from FEA were fitted to measured axial displacements by varying the aortic stiffness until convergence occurred, resulting in the subject specific aortic stiffness, which was found to correlate with diameter [30].

Magnetic resonance elastography (MRE) examines the propagation of shear waves through soft tissues. It has been used to investigate the correlation between aortic stiffness and aneurysm diameter finding significantly higher stiffness in AAA, than in both non-dilated vessel (in AAA cases) and age-matched healthy patients [31]. Patients with similar diameters had very different stiffness values, reinforcing the theory that maximum diameter alone is insufficient to differentiate between individual AAA's.

3.1.2 *Ex Vivo* Testing

Uniaxial tensile tests (UTTs) have been widely used to characterise the mechanical properties of aortic tissue *ex vivo*. Measurements are frequently performed in longitudinal and circumferential orientations to allow for anisotropy. There are well documented inconsistencies in the reporting of stress–strain behaviour derived from UTTs in the literature due to the different methods employed to calculate 'stress' and 'strain'. This can make

Table 1 Experimental studies investigating uniaxial tensile testing in AAA tissue

Study	Year	Testing method	Orientation	Control	Cases	Biomechanical measure	Control (KPa)	Cases (KPa)	P
He and Roach [33]	1994	Uniaxial	Longitudinal	5 AA	7 AAA	Stiffness	–	–	–
Raghavan et al. [34]	1996	Uniaxial	Longitudinal	7 AA	45 AAA	Failure stress	2014 ± 394	864 ± 102	<0.0005
Vorp et al. [40]	2001	Uniaxial	Circumferential	7 ILT < 4 mm	7 ILT > 4 mm	Failure stress	2160 ± 340	1380 ± 190	<0.05
Thubrikar et al. [91]	2001	Uniaxial	Longitudinal	–	5 AAA Lateral	Yield stress	–	510 ± 140	–
			Circumferential	–	Lateral	Yield stress	–	730 ± 220	–
			Longitudinal	–	Anterior	Yield stress	–	380 ± 180	–
			Circumferential	–	Anterior	Yield stress	–	520 ± 200	–
			Longitudinal	–	Posterior	Yield stress	–	470 ± 300	–
			Circumferential	–	Posterior	Yield stress	–	450 ± 140	–
Di Martino et al. [38]	2006	Uniaxial	Circumferential	16 AAA	9 rAAA	Failure stress	820 ± 90	540 ± 60	0.04
Raghavan et al. [92]	2006	Uniaxial	Longitudinal	–	4 AAA	Failure Stress	–	1266	–
Monteiro et al. [37]	2014	Uniaxial	Longitudinal	25 AAA < 55 mm diameter	65 AAA > 55 mm diameter	Failure stress	770 (533–1117)	1030 (757–1444)	0.027

Values are given as median ± IQR or mean (standard deviation)

AA represents abdominal aorta, AAA abdominal aortic aneurysm, rAAA ruptured abdominal aortic aneurysm, ILT intraluminal thrombus.

it difficult to compare results across studies [32]. Table 1 summarises experimental studies on human tissue since 1994. Aneurysmal tissue has been shown to be stiffer [33] and weaker [34, 35] than control. When separated into layers the adventitia was found to be significantly weaker in AAA, whilst the media was not significantly different [36]. Larger AAAs (>5.5 cm maximum diameter) were found to have higher failure properties than smaller AAAs (<5.5 cm) [37]; tissue from ruptured AAAs has been found to be both weaker [38] and not significantly different [39] from unruptured tissue; and AAA wall underlying thick ILT has been found to be weaker than that underlying thin ILT [40].

UTT can provide useful information regarding strength and stiffness but it is unable to replicate in vivo loading conditions. A fundamental goal in constitutive modelling is to be able to predict the mechanical behaviour of a tissue under its loading state [41]. Biaxial tensile testing (BTT) allows a 2D stress state, and is sufficient to develop constitutive relations. A description of BTT of AAA tissue is beyond the scope of this review but further details can be found in [42, 43].

3.2 Microscale

Macroscale testing is able to provide data regarding the global material properties of a tissue. By implementing

higher-resolution testing methods, it is possible to measure localised mechanical properties. This is especially useful for heterogeneous biological tissues, where they can be used to measure the mechanical properties of discrete tissue components.

3.2.1 Nanoindentation

Nanoindentation was originally developed to characterise engineering materials. The testing set up and principles are discussed in detail elsewhere [44, 45]. In brief, a rigid indenter, usually made of diamond, is used to probe the material under examination. The load and displacement are continuously recorded producing a load–unload curve from which the mechanical properties, usually hardness and elastic modulus, are calculated. Use of a sharp tip allows the elastic properties of hard (calcified) biological materials to be measured at the micron-length scale. However, soft biological materials present a challenge due to a high surface roughness and low stiffness making it difficult for the apparatus to register specimen contact prior to penetration. Thus the original technique has been modified to allow examination of soft biological materials, with use of a larger radius tip (100 µm) recommended to obtain reproducible results [46]. This necessarily compromises on spatial resolution.

Nanoindentation has been used to characterise the mechanical properties of non-human healthy aortic tissue specimens demonstrating that the specimen stiffness increases from the inner to outer portion of the vessel in both ferret [47] and porcine aorta [48]; stiffness increases with distance from the heart in ovine aorta [49] and is higher in the circumferential than axial orientation in porcine aorta [50] (Table 2).

Nanoindentation has been shown to be useful when used to probe aneurysmal human thoracic tissue [51, 52]. It has also been used on aneurysmal abdominal aorta. Meekel et al. performed indentations in the radial orientation on the intima (in-to-out [I-M]), adventitia (out-to-in [A-M]) and media (in-to-out [M-A] and out-to-in [M-I]) to establish the micromechanical properties of the individual aortic layers [53]. Contrary to previous findings from macroscale mechanical testing using imaging [30, 31], aneurysmal degeneration was associated with a reduced elastic modulus (reduced stiffness) in each layer except the adventitia, where it was non-significantly stiffer. This discrepancy may be because the aforementioned imaging studies are only able to measure a proxy of tissue stiffness, and even then, only of the whole composite structure including ILT and calcification, which were removed by Meekel et al. [53].

3.2.2 Scanning Acoustic Microscopy (SAM)

SAM is an imaging technique capable of providing both histological and mechanical information of in vitro biological specimens. The image contrast is derived from differences in the speed of propagation of acoustic waves through the tissue, which is related to the

Young's modulus. It is distinct from PWV and is able to measure the stiffness of separate tissue components. Detailed account of SAM is beyond the scope of this review but SAM has been applied to AAA tissue, and compared with atherosclerotic tissue. The only significant finding was of a slower wave speed and therefore lower elasticity in the intima of aneurysmal tissue [54].

3.3 Nanoscale

3.3.1 Atomic Force Microscopy (AFM)

AFM involves use of a nanometre-scale sharp probe mounted on a compliant cantilever. This tip is brought to the sample surface, with forces between sample and tip resulting in deflection of the cantilever. The deflection is measured by a laser light reflected off the cantilever upper surface to a photodetector. AFM is not only able to measure the mechanical properties at the nanoscale but it can also provide high spatial resolution images of tissue ultrastructure.

AFM has been used on atherosclerotic human abdominal [55] and healthy porcine thoracic [56] aorta, demonstrating that the elastin-rich lamellae are significantly stiffer than the interlamellar zones when a low strain compressive force is applied. Lindeman et al. applied AFM to human control and aneurysmal tissue from degenerative AAA [57]. AFM was used to probe the adventitia using both a sharp (20 nm) and blunter ball (10 μm) tip, theoretically allowing testing of individual fibres and tissue composite respectively. In control aorta, the response to indentation was the same regardless of tip diameter. In AAA, the sharp tip

Table 2 Studies utilising nanoindentation to investigate the mechanical properties of non-human aortic tissue

Study, year	Subject	Tissue	Indenter tip	Testing regime	Main findings
Akhtar et al. 2009 [47]	Ferret	DTA	10 μm Conospherical	Axial direction across full thickness of vessel	Linear decrease in E (stiffness) from adventitia (30 MPa) to intima (8 MPa)
Hemmasizadeh et al. 2012 [48]	Porcine	DTA	10 μm Conical	Axial direction across full thickness of vessel, at three levels along DTA	Outer half (adventitia) significantly stiffer (70.27 ± 2.47 kPa) than inner half (media) (60.32 ± 1.65 kPa)
Panpho et al. 2016 [49]	Ovine	Aorta, from root to coeliac axis	100 μm cylindrical flat punch	Radial direction on intimal and adventitial surface Circumferential direction to media	Linear increase in stiffness with distance from heart, which correlates with biochemical changes
Kermani et al. 2017 [50]	Porcine	DTA	10 μm Conical	Performed in 3 orientations; axial and circumferential (across full thickness of vessel) and radial from lumen. Specimens taken from 3 levels along DTA	E higher in circumferential than axial direction i.e. tissue demonstrates anisotropy

DTA indicates descending thoracic aorta, E Young's modulus, G' shear storage modulus, G'' shear loss modulus, MPa megapascals, kPa kilopascals, μm micrometre

registered very low stiffness, whereas the ball tip, registered much stiffer tissue. It is possible that in AAA there is a loss of interconnections which normally allow the tissue to behave as a coherent network, enabling the sharp tip to push fibres aside leading to lower resistance.

4 Intraluminal Thrombus (ILT)

ILT is present in 75% of AAA [58]. It is a three-dimensional fibrin structure consisting of blood proteins, blood cells, platelets and cellular debris, which accumulates in AAA in regions of low oscillatory shear index [59]. Its accumulation maintains physiological blood pressure and velocity in the expanding lumen. In patients undergoing AAA repair without evidence of frank aneurysm leak, the presence of a high attenuating peripheral crescent on pre-operative unenhanced CT (so-called ‘crescent sign’) was 77% sensitive and 93% specific for aneurysm ‘complications’ discovered during repair [60]. Thrombus from patients with the crescent sign and AAA rupture was characterised by clefts of seeping blood, which were not identified in unruptured AAA not demonstrating crescent sign [61]. Thus, ILT failure is thought to precede AAA rupture. Indeed, circumferential stress in a pressurised thick-walled tube is highest and lowest at the inner and outer edges, respectively [62].

4.1 Structure

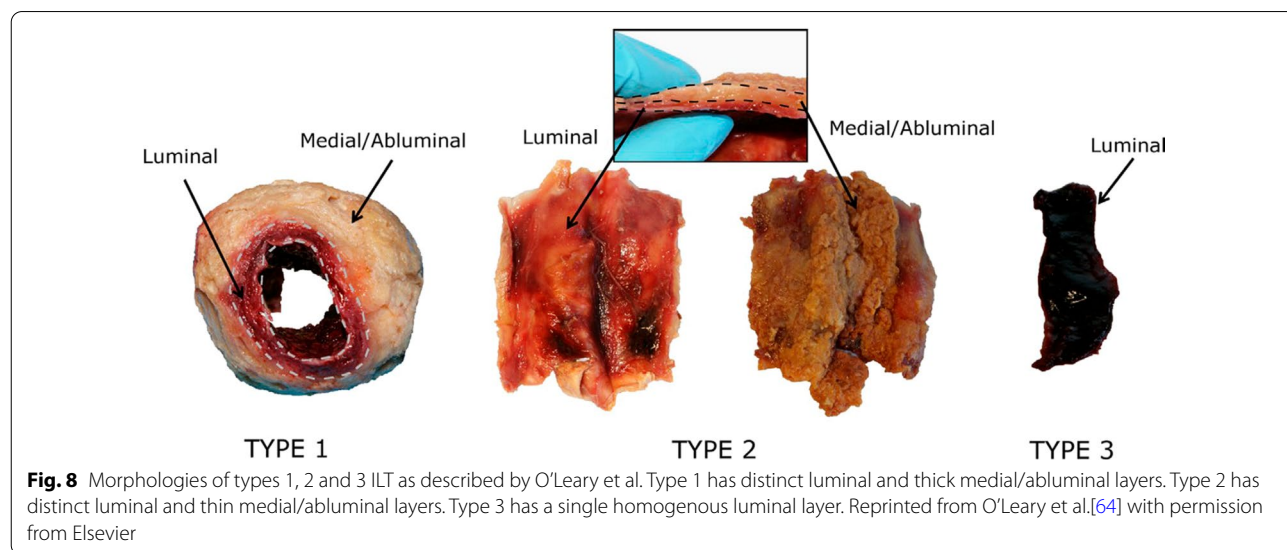
Initially thrombus is characterised by erythrocytes, platelets, thrombocytes and leucocytes embedded within a loose fibrin network. As it evolves, a secondary fibrin network of thick fibrin fibres forms through loss of erythrocytes and accumulation of platelets. A well-organised ILT structure can be described by three individual layers:

luminal (red), medial (white) and abluminal (brown), which can be differentiated histologically. The innermost and freshest ‘luminal layer’ is characterised by fibrin fibres arranged into thick bundles with fine secondary structures cross-linking them. In the medial layer, some fibres are degenerated, whereas in the abluminal layer, all fibres are degenerated with no coherent structure [63]. Not all thrombus is well-organised and three distinct morphologies have been described based on visual inspection and mechanical properties (Fig. 8) [64].

The ILT is traversed by canaliculi allowing passage of fluid and cells [65]. Gasser et al. used automatic image processing to examine the micro structure of histological slices from 7 ILT specimens harvested from human AAA [66]. They noted that the ratio of pore to ligament area reduced from the luminal (23.28% ± 4.03%) to the abluminal (19.59% ± 5.31%) layer. The abluminal layer exhibited more large pores and fewer small pores compared to the luminal and medial layers. Furthermore, pore orientation in the luminal layer tended to be towards the circumferential direction, whilst in the abluminal layer there was no preferred orientation, explaining the anisotropic and isotropic mechanical properties of these respective layers seen in some studies [64, 67].

4.2 Mechanical Testing

ILT is thought to affect the underlying aortic wall in multiple ways. Tanios et al. demonstrated that amount of types I, III and total collagen correlated negatively with increasing ILT thickness. They concluded that ILT may act to cushion the underlying aortic wall, thereby reducing wall stress and the need for compensatory collagen synthesis [68]. This was based on extrapolation from the observation that collagen content was



positively correlated with wall stress and failure tension. ILT has been shown to reduce wall stress in numerous computational studies [68–72] with the size of the effect depending on the shape of the aneurysm and the material properties of the thrombus. However, in one of the few experimental studies, Schurink et al. demonstrated that the pressure measured within ILT of AAA correlated with that measured in the radial artery, implying that ILT does not reduce the pressure (and therefore wall stress) on the underlying aortic wall [73]. This would account for the clinical observation that AAAs treated by iliac ligation and extra-anatomical bypass—inducing thrombosis in the aneurysm—can still rupture post-operatively [74–76]. One explanation for a reduction in wall stress despite transmitting systemic pressure to the aortic wall is provided by Thubrikar et al. who found experimentally that the longitudinal and circumferential strains induced by pressurising explanted AAA were significantly higher after removal of the thrombus [77], indicating that adherent ILT reinforces the AAA wall. Polzer et al. demonstrated this computationally by modelling the ILT as a poroelastic material [78].

Growth of ILT has been associated with aneurysm growth and rupture [79, 80]. It has been shown to be a reservoir for proteases with known activity against ECM proteins (albeit, the majority of the active proteases were found in the luminal layer, whilst the abluminal layer contained predominantly inactive forms due to presence of inhibitors) [81]. The wall adjacent to ILT has been shown to be thinner, contain fewer elastin fibres, fewer SMCs, and more apoptotic nuclei with clusters of inflammatory cells than wall adjacent to free flowing blood [82]. Vorp et al. demonstrated that aortic wall adjacent to thick ILT (>4 mm) was significantly weaker than tissue adjacent to thin ILT (<4 mm) in the same patient. Tissue from thick ILT areas showed a higher degree of inflammation and neovascularisation [40]. These changes were attributed to relative hypoxia by demonstrating a significantly lower partial pressure of oxygen (PaO_2) in the wall of patients with thick ILT [40]. Koole et al. demonstrated that ILT accumulation is positively correlated with MMP (matrix metalloproteinase)-2 content in the aortic wall, even after multivariable analysis [83], whilst Erdozain et al. demonstrated that SMCs secrete more MMP-2 under hypoxic conditions [84]. Thus, although ILT has been shown to reduce computational wall stress, it also has a deleterious effect on the underlying wall strength. Whether this is a direct effect due to hypoxia, an indirect effect due to reduction in wall stress, or a combination of both, remains uncertain.

Studies using FEA for patient specific rupture risk indices, such as PWS and rupture potential index (RPI), necessarily make several modelling assumptions, either

because it is impossible or impractical to use patient-specific values. Often, ILT is either excluded entirely or given homogenous material properties. Martufi et al. demonstrated the importance of including realistic material parameters for ILT, as well as aortic wall thickness, in an FEA model of rupture risk [85]. Tensile testing was used to establish the tissue strength and material properties of tissue taken from AAA patients. This tissue was categorised into 4 groups depending on wall and ILT thickness (thick or thin). The strongest tissue was found in the thin wall, thin thrombus group (772 ± 295 kPa); thick wall, thick thrombus was the weakest (334 ± 254 kPa). A patient-specific wall and ILT geometry was segmented creating a mesh for FEA. Each wall element was given an accurate wall thickness, and material properties based on the results from tensile testing. The generated PWS was 311 kPa. Further simulations disregarding ILT; using constant wall thickness; and using homogenous material properties for the wall resulted in significant changes in the location and magnitude of the PWS obtained, highlighting the importance of including ILT and its effect on the underlying aortic wall in FEA simulations.

Numerous studies have investigated the mechanical properties of human abdominal aortic ILT. A representative sample are summarised in Table 3. It is difficult to directly compare these due to differences in testing methods and analysis. In general, the elastic modulus obtained relates to the method of testing, with studies using rheometry [86] giving the lowest values, followed by studies using compression testing [87], and studies using tensile testing [69] giving the highest. However, the trends seen within the studies are similar. In summary, stiffness and strength decrease from the luminal to abluminal side (i.e. non-homogeneity), whereas the viscoelastic properties do not vary significantly [88]. ILT displays a degree of nonlinearity on biaxial tensile testing in both circumferential and longitudinal orientations, with this decreasing from luminal to abluminal layers [64]. The difference between the longitudinal and circumferential directions is minimal (i.e. isotropy) in the medial and abluminal layers but anisotropy has been demonstrated in the luminal layer [66, 67]. Two authors have investigated the regional heterogeneity of ILT- Celi et al. using uniaxial testing [89] and O’Leary et al. [64] using biaxial testing. Both found that the posterior region was stiffer than anterior. Tong et al. provide a comprehensive review of the structure, mechanics and histology of ILT [65].

Slaboch et al. [90] first used nanoindentation to investigate the mechanical properties of thrombi. They created murine thrombi and performed nanoindentation with a 1.75 mm flat punch cylindrical tip. Elastic contact theory was used to calculate the elastic modulus from the linear loading curve, with the result (55.1 ± 12.1 kPa) being

Table 3 Studies examining mechanical properties of ILT tissue

Study	Year	Patients (specimens)	Testing method	Stress	Strain	Relation	Description of specimens (number)	Strength mean (SD)		Stiffness mean (SD)	
								Measure	Result (KPa)	Measure	Result (KPa)
DiMartino et al. [69]	1998	6 (21)	UJT	Engineering	Engineering	Linear	Circumferential (21)	Ultimate Stress	85 (47)	Young's Modulus	131 (64)
Wang et al. [63]	2001	14 (50)	UJT	Cauchy	Engineering	Hyperelastic	Luminal (28) Longitudinal (14) Circumferential (14) Medial (22) Longitudinal (11) Circumferential (11)	Ultimate Stress	520 (70) 540 (70)	Maximum Tangential Modulus	540 (70) 570 (70)
Vande Geest et al. [93]	2006	9 (9)	BTT	Second Piola-Kirchhoff	Green	Linear	Luminal (9) Longitudinal (9) Circumferential (9)	NA—authors measured peak stretch at 40 N/m		Maximum Tangential Modulus	231 (29) 201 (16)
Hinnen et al. [87]	2007	6 (10)	DMA compression	NA	NA	Linear	All (10) Luminal (4) Lateral (4)	NA		Young's Modulus	~38 (15) ~31 (15) ~41 (15)
Gasser et al. [62]	2008	8 (112)	UJT	Cauchy	–	Linear	Circumferential (24) Luminal Medial Abluminal	Ultimate Stress	156.5 (57.9) 92 (37.5) 47.7 (22.9)	Young's Modulus	62.9 (19.2) 47.5 (14.9) 41.5 (15.4)
Tong et al. [67]	2011	43 (67)	BTT	Cauchy	Cauchy	–	Luminal 'Anisotropic' (10) Circumferential Longitudinal Luminal 'Isotropic' (23) Circumferential Longitudinal Medial (22) Circumferential Longitudinal Abluminal (12) Circumferential Longitudinal	Engineering stress causing rupture	60.5 (6.2)	Tangential Modulus at 20 kPa	208 (55) 291 (69) 189 (48) 206 (71) 137 (39) 145 (47) 27.9 (4.5)

consistent with others authors using compression to establish the mechanical properties of thrombi [87].

As ILT structure varies histologically, from the luminal (newer) to the abluminal (older) surface, it is possible that the material properties vary throughout its thickness. Van Dam et al. measured the material properties of ILT taken from 7 AAA patients using rheometry. They found that the variations found within one thrombus are of the same order of magnitude as found between patients. Accordingly, they concluded that the same material parameters may be used to describe all thrombi [88].

5 Conclusions

The maximum diameter threshold for aneurysm repair has been shown to be inferior to biomechanically based models for rupture risk assessment. To date, these models have utilised average material properties obtained from macroscale mechanical testing. It has been demonstrated that aneurysmal degeneration involves drastic structural changes and remodelling at the microscale. It is possible, using novel applications of high-resolution engineering techniques such as nanoindentation and AFM, to measure the micromechanical properties of ex vivo abdominal aortic tissue. These measurements could be correlated with biochemical assays and histological assessment to develop more realistic constitutive relations and material parameters for use in finite element simulations, which could further improve and personalise rupture risk prediction.

Abbreviations

A: Adventitia; AA: Abdominal aorta; AAA: Abdominal aortic aneurysm; AL: Abluminal layer; AFM: Atomic force microscopy; BTT: Biaxial tensile test; Cyt: Cytoplasm; DMA: Dynamic mechanical analysis; DTA: Descending thoracic aorta; E: Young's modulus; ECM: Extracellular matrix; EL: Elastic lamellae; EP: Elastin Pores; ES: Elastin struts; EVAR: Endovascular aneurysm repair; FEA: Finite element analysis; G': Shear storage modulus; G'': Shear loss modulus; GAG: Glycosaminoglycan; I: Intima; ILT: Intraluminal thrombus; kPa: Kilopascal; LL: Luminal layer; M: Media; MALDI-IMS: Matrix-assisted laser desorption/ionisation imaging mass spectrometry; MMP: Matrix metalloproteinase; MRE: Magnetic resonance elastography; N: Nuclei; NA: Not applicable; OSR: Open surgical repair; PaO₂: Partial pressure of oxygen; PG: Proteoglycan; PWS: Peak wall stress; PWW: Pulse wave velocity; rAAA: Ruptured abdominal aortic aneurysm; RPI: Rupture potential index; SAM: Scanning acoustic microscopy; SEM: Scanning electron microscopy; SMC: Smooth muscle cell; TG: Triglyceride; US: Ultrasound; UTT: Uniaxial tensile test.

Author contributions

MH performed the literature search and composed manuscript. All authors read and approved the final manuscript.

Funding

This research did not receive any specific grant from funding agencies in the public, commercial, or not-for-profit sectors.

Availability of Data and Materials

Not applicable.

Declarations

Conflict of Interest

The authors declare that they have no competing interests.

Ethics Approval and Consent to Participate

Not applicable.

Consent for Publication

Not applicable.

Author details

¹Mechanical, Materials and Aerospace Engineering, University of Liverpool, Liverpool, UK. ²Liverpool Vascular and Endovascular Service, Liverpool University Hospitals NHS Foundation Trust, Liverpool, UK. ³Institute of Systems, Molecular and Integrative Biology, University of Liverpool, Liverpool, UK. ⁴Cardiothoracic Surgery, Liverpool Heart and Chest Hospital NHS Foundation Trust, Liverpool, UK.

Received: 6 December 2021 Accepted: 8 February 2022

Published online: 7 March 2022

References

- Oliver-Williams C, Sweeting MJ, Turton G, Parkin D, Cooper D, Rodd C, et al. Lessons learned about prevalence and growth rates of abdominal aortic aneurysms from a 25-year ultrasound population screening programme. *Br J Surg*. 2018;105:68–74. <https://doi.org/10.1002/bjs.10715>.
- Vorp DA, Vande Geest JP. Biomechanical determinants of abdominal aortic aneurysm rupture. *Arterioscler Thromb Vasc Biol*. 2005;25:1558–66. <https://doi.org/10.1161/01.ATV.0000174129.77391.55>.
- Qadura M, Pervaiz F, Harlock JA, Al-Azzoni A, Farrokhhyar F, Kahnemou K, et al. Mortality and reintervention following elective abdominal aortic aneurysm repair. *J Vasc Surg*. 2013. <https://doi.org/10.1016/j.jvs.2013.02.013>.
- Glimåker H, Holmberg L, Elvin A, Nybacka O, Almgren B, Björck CG, et al. Natural history of patients with abdominal aortic aneurysm. *Eur J Vasc Surg*. 1991;5:125–30. [https://doi.org/10.1016/S0950-821X\(05\)80675-9](https://doi.org/10.1016/S0950-821X(05)80675-9).
- Wanhainen A, Verzini F, Van Herzele I, Allaire E, Bown M, Cohnert T, et al. European Society for Vascular Surgery (ESVS) 2019 clinical practice guidelines on the management of abdominal aorto-iliac artery aneurysms. *Eur J Vasc Endovasc Surg*. 2019;57:8–93. <https://doi.org/10.1016/j.ejvs.2018.09.020>.
- Filardo G, Powell JT, Martinez MAM, Ballard DJ. Surgery for small asymptomatic abdominal aortic aneurysms. *Cochrane Database Syst Rev*. 2015. <https://doi.org/10.1002/14651858.CD001835.pub4>.
- Laine MT, Vääntinen T, Kantonen I, Halmesmäki K, Weselius EM, Laukonen S, et al. Rupture of abdominal aortic aneurysms in patients under screening age and elective repair threshold. *Eur J Vasc Endovasc Surg*. 2016;51:511–6. <https://doi.org/10.1016/j.ejvs.2015.12.011>.
- Brady AR, Thompson SG, Fowkes FGR, Greenhalgh RM, Powell JT. Abdominal aortic aneurysm expansion: risk factors and time intervals for surveillance. *Circulation*. 2004;110:16–21. <https://doi.org/10.1161/01.CIR.0000133279.07468.9f>.
- Fillinger MF, Raghavan ML, Marra SP, Cronenwett JL, Kennedy FE. In vivo analysis of mechanical wall stress and abdominal aortic aneurysm rupture risk. *J Vasc Surg*. 2002;36:589–97. <https://doi.org/10.1067/mva.2002.125478>.
- Fillinger MF, Marra SP, Raghavan ML, Kennedy FE. Prediction of rupture risk in abdominal aortic aneurysm during observation: wall stress versus diameter. *J Vasc Surg*. 2003;37:724–32. <https://doi.org/10.1067/mva.2003.213>.
- Scotti CM, Jimenez J, Muluk SC, Finol EA. Wall stress and flow dynamics in abdominal aortic aneurysms: finite element analysis vs fluid-structure interaction. *Comput Methods Biomech Biomed Engin*. 2008;11:301–22. <https://doi.org/10.1080/10255840701827412>.
- Venkatasubramaniam AK, Fagan MJ, Mehta T, Mylankal KJ, Ray B, Kuhan G, et al. A comparative study of aortic wall stress using finite element

- analysis for ruptured and non-ruptured abdominal aortic aneurysms. *Eur J Vasc Endovasc Surg.* 2004;28:168–76. <https://doi.org/10.1016/j.ejvs.2004.03.029>.
13. Harkness M, Harkness R, McDonald D. The collagen and elastin content of the arterial wall. *J Physiol.* 1955;127:33–4.
 14. Theocharis AD, Tsolakis I, Hjerpe A, Karamanos NK. Human abdominal aortic aneurysm is characterized by decreased versican concentration and specific downregulation of versican isoform V 0. *Atherosclerosis.* 2001;154:367–76.
 15. Sakalihan N, Heyeres A, Nusgens BV, Limet R, Lapière CM. Modifications of the extracellular matrix of aneurysmal abdominal aortas as a function of their size. *Eur J Vasc Surg.* 1993;7:633–7. [https://doi.org/10.1016/S0950-821X\(05\)80708-X](https://doi.org/10.1016/S0950-821X(05)80708-X).
 16. Theocharis AD, Tsolakis I, Tseggenidis T, Karamanos NK. Human abdominal aortic aneurysm is closely associated with compositional and specific structural modifications at the glycosaminoglycan level. *Atherosclerosis.* 1999;145:359–68. [https://doi.org/10.1016/S0021-9150\(99\)00117-3](https://doi.org/10.1016/S0021-9150(99)00117-3).
 17. Didangelos A, Yin X, Mandal K, Saje A, Smith A, Xu Q, et al. Extracellular matrix composition and remodeling in human abdominal aortic aneurysms: a proteomics approach. *Mol Cell Proteomics.* 2011. <https://doi.org/10.1074/MCP.M111.008128>.
 18. Niestrawska JA, Viertler C, Regitnig P, Cohnert TU, Sommer G, Holzapfel GA. Microstructure and mechanics of healthy and aneurysmal abdominal aortas: experimental analysis and modelling. *J R Soc Interface.* 2016;13:20160620. <https://doi.org/10.1098/rsif.2016.0620>.
 19. Schulze-Bauer CAJ, Mörth C, Holzapfel GA. Passive biaxial mechanical response of aged human iliac arteries. *J Biomech Eng.* 2003. <https://doi.org/10.1115/1.1574331>.
 20. Holzapfel GA, Sommer G, Gasser CT, Regitnig P. Determination of layer-specific mechanical properties of human coronary arteries with non-atherosclerotic intimal thickening and related constitutive modeling. *Am J Physiol Hear Circ Physiol.* 2005;289:2048–58. <https://doi.org/10.1152/ajpheart.00934.2004>.
 21. O'Connell MK, Murthy S, Phan S, Xu C, Buchanan JA, Spilker R, et al. The three-dimensional micro- and nanostructure of the aortic medial lamellar unit measured using 3D confocal and electron microscopy imaging. *Matrix Biol.* 2008;27:171–81. <https://doi.org/10.1016/j.matbio.2007.10.008>.
 22. Holzapfel GA, Gasser TC, Ogden RW. A new constitutive framework for arterial wall mechanics and a comparative study of material models. *J Elast.* 2000;61:1–48. <https://doi.org/10.1023/A:1010835316564>.
 23. Garoffolo G, Pesce M. Mechanotransduction in the cardiovascular system: from developmental origins to homeostasis and pathology. *Cells.* 2019;8:1607. <https://doi.org/10.3390/cells8121607>.
 24. Raspanti M, Protasoni M, Manelli A, Guizzardi S, Mantovani V, Sala A. The extracellular matrix of the human aortic wall: Ultrastructural observations by FEG-SEM and by tapping-mode AFM. *Micron.* 2006;37:81–6. <https://doi.org/10.1016/j.micron.2005.06.002>.
 25. Niestrawska JA, Regitnig P, Viertler C, Cohnert TU, Babu AR, Holzapfel GA. The role of tissue remodeling in mechanics and pathogenesis of abdominal aortic aneurysms. *Acta Biomater.* 2019;88:149–61. <https://doi.org/10.1016/j.actbio.2019.01.070>.
 26. Tanaka H, Zaima N, Sasaki T, Yamamoto N, Inuzuka K, Sano M, et al. Imaging mass spectrometry reveals a unique distribution of triglycerides in the abdominal aortic aneurysmal wall. *J Vasc Res.* 2015;52:127–35. <https://doi.org/10.1159/000439169>.
 27. Watt HC, Law MR, Wald NJ, Craig WY, Ledue TB, Haddow JE. Serum triglyceride: a possible risk factor for ruptured abdominal aortic aneurysm. *Int J Epidemiol.* 1998;27:949–52. <https://doi.org/10.1093/ije/27.6.949>.
 28. Majewski W, Stanišić M, Pawlaczyk K, Marszałek A, Seget M, Biczysko W, et al. Morphological and mechanical changes in juxtarenal aortic segment and aneurysm before and after open surgical repair of abdominal aortic aneurysms. *Eur J Vasc Endovasc Surg.* 2010;40:202–8. <https://doi.org/10.1016/j.ejvs.2010.04.015>.
 29. Li RX, Luo J, Balaram SK, Chaudhry FA, Shahmirzadi D, Konofagou EE. Pulse wave imaging in normal, hypertensive and aneurysmal human aortas in vivo: a feasibility study. *Phys Med Biol.* 2013;58:4549–62. <https://doi.org/10.1088/0031-9155/58/13/4549>.
 30. Van Disseldorp EMJ, Petterson NJ, Van De Vosse FN, Van Sambeek MRHM, Lopata RGP. Quantification of aortic stiffness and wall stress in healthy volunteers and abdominal aortic aneurysm patients using time-resolved 3D ultrasound: a comparison study. *Eur Heart J Cardiovasc Imaging.* 2019;20:185–91. <https://doi.org/10.1093/ehjci/jej051>.
 31. Kolipaka A, Illapani VSP, Kenyhercz W, Dowell JD, Go MR, Starr JE, et al. Quantification of abdominal aortic aneurysm stiffness using magnetic resonance elastography and its comparison to aneurysm diameter. *J Vasc Surg.* 2016;64:966–74. <https://doi.org/10.1016/j.jvs.2016.03.426>.
 32. Khanafer K, Schlicht MS, Berguer R. How should we measure and report elasticity in aortic tissue? *Eur J Vasc Endovasc Surg.* 2013;45:332–9. <https://doi.org/10.1016/j.ejvs.2012.12.015>.
 33. He CM, Roach MR. The composition and mechanical properties of abdominal aortic aneurysms. *J Vasc Surg.* 1994;20:6–13. [https://doi.org/10.1016/0741-5214\(94\)90169-4](https://doi.org/10.1016/0741-5214(94)90169-4).
 34. Raghavan ML, Webster MW, Vorp DA. Ex vivo biomechanical behavior of abdominal aortic aneurysm: assessment using a new mathematical model. *Ann Biomed Eng.* 1996;24:573–82. <https://doi.org/10.1007/BF02684226>.
 35. Vallabhaneni SR, Gilling-Smith GL, How TV, Carter SD, Brennan JA, Harris PL. Heterogeneity of tensile strength and matrix metalloproteinase activity in the wall of abdominal aortic aneurysms. *J Endovasc Ther.* 2004;11:494–502. <https://doi.org/10.1583/04-1239-1>.
 36. Teng Z, Feng J, Zhang Y, Huang Y, Sutcliffe MPF, Brown AJ, et al. Layer- and direction-specific material properties, extreme extensibility and ultimate material strength of human abdominal aorta and aneurysm: a uniaxial extension study. *Ann Biomed Eng.* 2015;43:2745–59. <https://doi.org/10.1007/s10439-015-1323-6>.
 37. Tavares-Monteiro JA, Da Silva ES, Raghavan ML, Puech-Leão P, De Lourdes-Higuchi M, Otoch JP. Histologic, histochemical, and biomechanical properties of fragments isolated from the anterior wall of abdominal aortic aneurysms. *J Vasc Surg.* 2014;59:1393-401.e1-2. <https://doi.org/10.1016/j.jvs.2013.04.064>.
 38. Di Martino ES, Bohra A, Vande Geest JP, Gupta N, Makaroun MS, Vorp DA. Biomechanical properties of ruptured versus electively repaired abdominal aortic aneurysm wall tissue. *J Vasc Surg.* 2006;43:570–6. <https://doi.org/10.1016/j.jvs.2005.10.072>.
 39. Raghavan ML, Hanaoka MM, Kratzberg JA, de Higuchi ML, da Silva ES. Biomechanical failure properties and microstructural content of ruptured and unruptured abdominal aortic aneurysms. *J Biomech.* 2011;44:2501–7. <https://doi.org/10.1016/j.jbiomech.2011.06.004>.
 40. Vorp DA, Lee PC, Wang DHJ, Makaroun MS, Nemoto EM, Ogawa S, et al. Association of intraluminal thrombus in abdominal aortic aneurysm with local hypoxia and wall weakening. *J Vasc Surg.* 2001;34:291–9. <https://doi.org/10.1067/mva.2001.114813>.
 41. Sacks MS. Biaxial mechanical evaluation of planar biological materials. *J Elast.* 2000;61:199–246. <https://doi.org/10.1023/A:1010917028671>.
 42. Vande Geest JP, Sacks MS, Vorp DA. The effects of aneurysm on the biaxial mechanical behavior of human abdominal aorta. *J Biomech.* 2006;39:1324–34. <https://doi.org/10.1016/j.jbiomech.2005.03.003>.
 43. O'Leary SA, Healey DA, Kavanagh EG, Walsh MT, McGloughlin TM, Doyle BJ. The biaxial biomechanical behavior of abdominal aortic aneurysm tissue. *Ann Biomed Eng.* 2014;42:2440–50. <https://doi.org/10.1007/s10439-014-1106-5>.
 44. Oliver WC, Pharr GM. An improved technique for determining hardness and elastic modulus using load and displacement sensing indentation experiments. *J Mater Res.* 1992;7:1564–83. <https://doi.org/10.1557/JMR.1992.1564>.
 45. Akhtar R, Draper ER, Adams DJ, Hay J. Oscillatory nanoindentation of highly compliant hydrogels: a critical comparative analysis with rheometry. *J Mater Res.* 2018;33:873–83. <https://doi.org/10.1557/jmr.2018.62>.
 46. Ebenstein DM, Pruitt LA. Nanoindentation of soft hydrated materials for application to vascular tissues. *J Biomed Mater Res Part A.* 2004;69:222–32. <https://doi.org/10.1002/jbm.a.20096>.
 47. Akhtar R, Schwarzer N, Sherratt MJ, Watson REB, Graham HK, Trafford AW, et al. Nanoindentation of histological specimens: Mapping the elastic properties of soft tissues. *J Mater Res.* 2009;24:638–46. <https://doi.org/10.1557/jmr.2009.0130>.
 48. Hemmasizadeh A, Autieri M, Darvish K. Multilayer material properties of aorta determined from nanoindentation tests. *J Mech Behav Biomed Mater.* 2012;15:199–207. <https://doi.org/10.1016/j.jmbm.2012.06.008>.
 49. Panpho P, Geraghty B, Chim YH, Davies HA, Field ML, Madine J, et al. Macro- and micro-mechanical properties of the ovine aorta: correlation

- with regional variations in collagen, elastin and glycosaminoglycan levels. *Artery Res.* 2019;25:27–36. <https://doi.org/10.2991/artres.k.191114.003>.
50. Kermani G, Hemmasizadeh A, Assari S, Autieri M, Darvish K. Investigation of inhomogeneous and anisotropic material behavior of porcine thoracic aorta using nano-indentation tests. *J Mech Behav Biomed Mater.* 2017;69:50–6. <https://doi.org/10.1016/j.jmbbm.2016.12.022>.
 51. Davies HA, Caamaño-Gutiérrez E, Chim YH, Field M, Nawaytou O, Ressel L, et al. Idiopathic degenerative thoracic aneurysms are associated with increased aortic medial amyloid. *Amyloid.* 2019;26:148–55. <https://doi.org/10.1080/13506129.2019.1625323>.
 52. Chim YH, Davies HA, Mason D, Nawaytou O, Field M, Madine J, et al. Bicuspid valve aortopathy is associated with distinct patterns of matrix degradation. *J Thorac Cardiovasc Surg.* 2020;160:e239–57. <https://doi.org/10.1016/j.jtcvs.2019.08.094>.
 53. Meekel JP, Mattei G, Costache VS, Balm R, Blankensteijn JD, Yeung KK. A multilayer micromechanical elastic modulus measuring method in ex vivo human aneurysmal abdominal aortas. *Acta Biomater.* 2019;96:345–53. <https://doi.org/10.1016/j.actbio.2019.07.019>.
 54. Saijo Y, Miyakawa T, Sasaki H, Tanaka M, Nitta SI. Acoustic properties of aortic aneurysm obtained with scanning acoustic microscopy. *Ultrasonics.* 2004;42:695–8. <https://doi.org/10.1016/j.ultras.2003.11.023>.
 55. Rezvani-Sharif A, Tafazzoli-Shadpour M, Avolio A. Mechanical characterization of the lamellar structure of human abdominal aorta in the development of atherosclerosis: an atomic force microscopy study. *Cardiovasc Eng Technol.* 2019;10:181–92. <https://doi.org/10.1007/s13239-018-0370-1>.
 56. Matsumoto T, Goto T, Furukawa T, Sato M. Residual stress and strain in the lamellar unit of the porcine aorta: experiment and analysis. *J Biomech.* 2004;37:807–15. <https://doi.org/10.1016/j.jbiomech.2003.08.014>.
 57. Lindeman JHN, Ashcroft BA, Beenakker JWM, Van Es M, Koekkoek NBR, Prins FA, et al. Distinct defects in collagen microarchitecture underlie vessel-wall failure in advanced abdominal aneurysms and aneurysms in Marfan syndrome. *Proc Natl Acad Sci U S A.* 2010;107:862–5. <https://doi.org/10.1073/pnas.0910312107>.
 58. Choke E, Cockerill G, Wilson WRW, Sayed S, Dawson J, Loftus I, et al. A review of biological factors implicated in abdominal aortic aneurysm rupture. *Eur J Vasc Endovasc Surg.* 2005;30:227–44. <https://doi.org/10.1016/j.ejvs.2005.03.009>.
 59. O'Rourke MJ, McCullough JP, Kelly S. An investigation of the relationship between hemodynamics and thrombus deposition within patient-specific models of abdominal aortic aneurysm. *Proc Inst Mech Eng Part H J Eng Med.* 2012. <https://doi.org/10.1177/0954411912444080>.
 60. Mehard WB, Heiken JP, Sicard GA. High-attenuating crescent in abdominal aortic aneurysm wall at CT: a sign of acute or impending rupture. *Radiology.* 1994. <https://doi.org/10.1148/radiology.192.2.8029397>.
 61. Arita T, Matsunaga N, Takano K, Nagaoka S, Nakamura H, Katayama S, et al. Abdominal aortic aneurysm: rupture associated with the high-attenuating crescent sign. *Radiology.* 1997. <https://doi.org/10.1148/radiology.204.3.9280256>.
 62. Gasser TC, Görgülü G, Folkesson M, Swedenborg J. Failure properties of intraluminal thrombus in abdominal aortic aneurysm under static and pulsating mechanical loads. *J Vasc Surg.* 2008;48:179–88. <https://doi.org/10.1016/j.jvs.2008.01.036>.
 63. Wang DHJ, Makaroun M, Webster MW, Vorp DA. Mechanical properties and microstructure of intraluminal thrombus from abdominal aortic aneurysm. *J Biomech Eng.* 2001;123:536–9. <https://doi.org/10.1115/1.1411971>.
 64. O'Leary SA, Kavanagh EG, Grace PA, McGloughlin TM, Doyle BJ. The biaxial mechanical behaviour of abdominal aortic aneurysm intraluminal thrombus: classification of morphology and the determination of layer and region specific properties. *J Biomech.* 2014;47:1430–7. <https://doi.org/10.1016/j.jbiomech.2014.01.041>.
 65. Tong J, Holzapfel GA. Structure, mechanics, and histology of intraluminal thrombi in abdominal aortic aneurysms. *Ann Biomed Eng.* 2015;43:1488–501. <https://doi.org/10.1007/s10439-015-1332-5>.
 66. Gasser TC, Martufi G, Auer M, Folkesson M, Swedenborg J. Micromechanical characterization of intra-luminal thrombus tissue from abdominal aortic aneurysms. *Ann Biomed Eng.* 2010;38:371–9. <https://doi.org/10.1007/s10439-009-9837-4>.
 67. Tong J, Cohnert T, Regitnig P, Holzapfel GA. Effects of age on the elastic properties of the intraluminal thrombus and the thrombus-covered wall in abdominal aortic aneurysms: biaxial extension behaviour and material modelling. *Eur J Vasc Endovasc Surg.* 2011;42:207–19. <https://doi.org/10.1016/j.ejvs.2011.02.017>.
 68. Tanius F, Gee MW, Pelisek J, Kehl S, Biehler J, Grabher-Meier V, et al. Interaction of biomechanics with extracellular matrix components in abdominal aortic aneurysm wall. *Eur J Vasc Endovasc Surg.* 2015;50:167–74. <https://doi.org/10.1016/j.ejvs.2015.03.021>.
 69. Di Martino E, Mantero S, Inzoli F, Melissano G, Astore D, Chiesa R, et al. Biomechanics of abdominal aortic aneurysm in the presence of endoluminal thrombus: experimental characterisation and structural static computational analysis. *Eur J Vasc Endovasc Surg.* 1998;15:290–9. [https://doi.org/10.1016/S1078-5884\(98\)80031-2](https://doi.org/10.1016/S1078-5884(98)80031-2).
 70. Inzoli F, Boschetti F, Zappa M, Longo T, Fumero R. Biomechanical factors in abdominal aortic aneurysm rupture. *Eur J Vasc Surg.* 1993;7:667–74. [https://doi.org/10.1016/S0950-821X\(05\)80714-5](https://doi.org/10.1016/S0950-821X(05)80714-5).
 71. Wang DHJ, Makaroun MS, Webster MW, Vorp DA. Effect of intraluminal thrombus on wall stress in patient-specific models of abdominal aortic aneurysm. *J Vasc Surg.* 2002;36:598–604. <https://doi.org/10.1067/mva.2002.126087>.
 72. Di Martino ES, Vorp DA. Effect of variation in intraluminal thrombus constitutive properties on abdominal aortic aneurysm wall. *Stress.* 2003. <https://doi.org/10.1114/1.1581880>.
 73. Schurink GWH, Van Baalen JM, Visser MJT, Van Bockel JH. Thrombus within an aortic aneurysm does not reduce pressure on the aneurysmal wall. *J Vasc Surg.* 2000. <https://doi.org/10.1067/mva.2000.103693>.
 74. Ricotta JJ, Kirshner RL. Case report: late rupture of a thrombosed abdominal aortic aneurysm. *Surgery.* 1984;95:753–5.
 75. Schanzer H, Papa MC, Miller CM. Rupture of surgically thrombosed abdominal aortic aneurysm. *J Vasc Surg.* 1985. [https://doi.org/10.1016/0741-5214\(85\)90064-3](https://doi.org/10.1016/0741-5214(85)90064-3).
 76. Kwaan JHM, Dahl RK. Fatal rupture after successful surgical thrombosis of an abdominal aortic aneurysm. *Surgery.* 1984;95:235–7.
 77. Thubrikar MJ, Robicsek F, Labrosse M, Chervenkov V, Fowler BL. Effect of thrombus on abdominal aortic aneurysm wall dilation and stress. *J Cardiovasc Surg (Torino).* 2003;44:67–77.
 78. Polzer S, Gasser TC, Markert B, Bursa J, Skacel P. Impact of poroelasticity of intraluminal thrombus on wall stress of abdominal aortic aneurysms. *Biomed Eng Online.* 2012;1:1–13. <https://doi.org/10.1186/1475-925X-11-62>.
 79. Stenbaek J, Kalin B, Swedenborg J. Growth of thrombus may be a better predictor of rupture than diameter in patients with abdominal aortic aneurysms. *Eur J Vasc Endovasc Surg.* 2000. <https://doi.org/10.1053/ejvs.2000.1217>.
 80. Wolf YG, Thomas WS, Brennan FJ, Goff WG, Sise MJ, Bernstein EF. Computed tomography scanning findings associated with rapid expansion of abdominal aortic aneurysms. *J Vasc Surg.* 1994. [https://doi.org/10.1016/0741-5214\(94\)90277-1](https://doi.org/10.1016/0741-5214(94)90277-1).
 81. Folkesson M, Silveira A, Eriksson P, Swedenborg J. Protease activity in the multi-layered intra-luminal thrombus of abdominal aortic aneurysms. *Atherosclerosis.* 2011. <https://doi.org/10.1016/j.atherosclerosis.2011.05.002>.
 82. Kazi M, Thyberg J, Religa P, Roy J, Eriksson P, Hedin U, et al. Influence of intraluminal thrombus on structural and cellular composition of abdominal aortic aneurysm wall. *J Vasc Surg.* 2003;38:1283–92. [https://doi.org/10.1016/S0741-5214\(03\)00791-2](https://doi.org/10.1016/S0741-5214(03)00791-2).
 83. Koole L, Zandvoort HJA, Schoneveld A, Vink A, Vos JA, Van Den Hoogen LL, et al. Intraluminal abdominal aortic aneurysm thrombus is associated with disruption of wall integrity. *J Vasc Surg.* 2013;57:77–83. <https://doi.org/10.1016/j.jvs.2012.07.003>.
 84. Erdozain OJ, Pegrum S, Winrow VR, Horrocks M, Stevens CR. Hypoxia in abdominal aortic aneurysm supports a role for HIF-1 α and Ets-1 as drivers of matrix metalloproteinase upregulation in human aortic smooth muscle cells. *J Vasc Res.* 2011;48:163–70. <https://doi.org/10.1159/000318806>.
 85. Martufi G, Satriano A, Moore RD, Vorp DA, Di Martino ES. Local quantification of wall thickness and intraluminal thrombus offer insight into the mechanical properties of the aneurysmal aorta. *Ann Biomed Eng.* 2015. <https://doi.org/10.1007/s10439-014-1222-2>.
 86. Van Dam EA, Dams SD, Peters GWM, Rutten MCM, Schurink GWH, Buth J, et al. Determination of linear viscoelastic behavior of abdominal aortic aneurysm thrombus. *Biorheology.* 2006;43:695–707.

87. Hinnen JW, Rixen DJ, Koning OHJ, van Bockel JH, Hamming JF. Development of fibrinous thrombus analogue for in-vitro abdominal aortic aneurysm studies. *J Biomech*. 2007. <https://doi.org/10.1016/j.jbiomech.2006.01.010>.
88. Van Dam EA, Dams SD, Peters GWM, Rutten MCM, Schurink GWH, Buth J, et al. Non-linear viscoelastic behavior of abdominal aortic aneurysm thrombus. *Biomech Model Mechanobiol*. 2008. <https://doi.org/10.1007/s10237-007-0080-3>.
89. Celi S, Losi P, Berti S. Investigation on regional variation of intraluminal thrombus: a mechanical and histological study. *Bioinspired Biomim Nanobiomaterials*. 2012. <https://doi.org/10.1680/bbn.12.00006>.
90. Slaboch CL, Alber MS, Rosen ED, Ovaert TC. Mechano-rheological properties of the murine thrombus determined via nanoindentation and finite element modeling. *J Mech Behav Biomed Mater*. 2012;10:75–86. <https://doi.org/10.1016/j.jmbbm.2012.02.012>.
91. Thubrikar MJ, Labrosse M, Robicsek F, Al-Soudi J, Fowler B. Mechanical properties of abdominal aortic aneurysm wall. *J Med Eng Technol*. 2001;25:133–42. <https://doi.org/10.1080/03091900110057806>.
92. Raghavan ML, Kratzberg J, Castro-de-Tolosa EM, Hanaoka MM, Walker P, da Silva ES. Regional distribution of wall thickness and failure properties of human abdominal aortic aneurysm. *J Biomech*. 2006;39:3010–6. <https://doi.org/10.1016/j.jbiomech.2005.10.021>.
93. Vande Geest JP, Sacks MS, Vorp DA. A planar biaxial constitutive relation for the luminal layer of intra-luminal thrombus in abdominal aortic aneurysms. *J Biomech*. 2006;39:2347–54. <https://doi.org/10.1016/j.jbiomech.2006.05.011>.

Ready to submit your research? Choose BMC and benefit from:

- fast, convenient online submission
- thorough peer review by experienced researchers in your field
- rapid publication on acceptance
- support for research data, including large and complex data types
- gold Open Access which fosters wider collaboration and increased citations
- maximum visibility for your research: over 100M website views per year

At BMC, research is always in progress.

Learn more biomedcentral.com/submissions

